Zinc Phthalocyanine–Graphene Hybrid Material for Energy Conversion: Synthesis, Characterization, Photophysics, and Photoelectrochemical Cell Preparation

ARTICLE *in* THE JOURNAL OF PHYSICAL CHEMISTRY C · SEPTEMBER 2012

Impact Factor: 4.77 · DOI: 10.1021/jp305783v

8 AUTHORS, INCLUDING:

Nikolaos Karousis
National Hellenic Research Foundation
39 PUBLICATIONS **941** CITATIONS
SEE PROFILE

Kei Ohkubo
Osaka University
395 PUBLICATIONS **9,565** CITATIONS
SEE PROFILE

Angela Sastre-Santos
Universidad Miguel Hernández de Elche
107 PUBLICATIONS **2,278** CITATIONS
SEE PROFILE

THE JOURNAL OF PHYSICAL CHEMISTRY C

Article

pubs.acs.org/JPCC

Zinc Phthalocyanine–Graphene Hybrid Material for Energy Conversion: Synthesis, Characterization, Photophysics, and Photoelectrochemical Cell Preparation

Nikolaos Karousis,[†] Javier Ortiz,[‡] Kei Ohkubo,[∥] Taku Hasobe,*[,§] Shunichi Fukuzumi,*[,∥,⊥] Ángela Sastre-Santos,*[,‡] and Nikos Tagmatarchis*[,†]

[†]Theoretical and Physical Chemistry Institute, National Hellenic Research Foundation, 48 Vassileos Constantinou Avenue, Athens 116 35, Greece

[‡]Division de Química Orgánica, Instituto de Bioingeniería, Universidad Miguel Hernández, Elche 03202, Spain

[§]Department of Chemistry, Faculty of Science and Technology, Keio University, Yokohama, 223-8522, Japan

[∥]Department of Material and Life Science, Graduate School of Engineering, Osaka University, ALCA, Japan Science and Technology Agency (JST), Suita, Osaka, 565-0871, Japan

[⊥]Department of Bioinspired Science, Ewha Womans University, Seoul 120-750, Korea

Supporting Information

ABSTRACT: Graphene exfoliation upon tip sonication in *o*-dichlorobenzene (*o*-DCB) was accomplished. Covalent grafting of (2-aminoethoxy)(tri-*tert*-butyl) zinc phthalocyanine (ZnPc) to exfoliated graphene sheets was then achieved. The newly formed ZnPc–graphene hybrid material was found to be soluble in common organic solvents without any precipitation for several weeks. Application of diverse spectroscopic techniques verified the successful formation of the ZnPc–graphene hybrid material, while thermogravimetric analysis revealed the amount of ZnPc loading onto graphene. Microscopy analysis based on AFM and TEM was applied to probe the morphological characteristics and to investigate the exfoliation of graphene sheets. Efficient fluorescence quenching of ZnPc in the ZnPc–graphene hybrid material suggested that photoinduced events occur from the photoexcited ZnPc to exfoliated graphene. The dynamics of the photoinduced electron transfer was evaluated by femtosecond transient absorption spectroscopy, thus revealing the formation of transient species such as $ZnPc^{\bullet+}$, yielding the charge-separated state $ZnPc^{\bullet+}$–$graphene^{\bullet-}$. Finally, the ZnPc–graphene hybrid material was integrated into a photoactive electrode of an optical transparent electrode (OTE) cast with nanostructured SnO_2 films (OTE/SnO_2), which exhibited stable and reproducible photocurrent responses, and the incident photon-to-current conversion efficiency was determined.

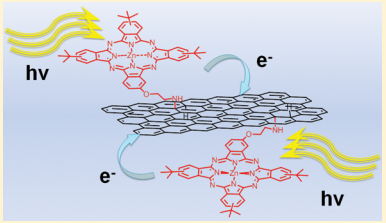

INTRODUCTION

Graphene is an outstanding material, consisting of a two-dimensional (2D) single layer of sp^2-hybridized carbon atoms bonded together in a hexagonal "honeycomb" lattice and presents remarkable mechanical and thermal properties.[1,2] Moreover, electrons can travel up to micrometers on the graphene plane without being scattered off by defects sites, giving to graphene a remarkably high electrical conductivity.[3−7] These exceptional properties of graphene make it an ideal candidate in the construction of transparent conducting electrodes that could be used in energy conversion and storage systems.[8,9] Additionally, both sides of graphene's double-sided plane are free to participate in a great plethora of organic reactions, offering an alternative approach to the control of its electronic properties.[10,11]

Fabrication of graphene onto substrates requires exfoliation in the form of a single or even a few layers as well as fine dispersion in common organic solvents, while at the same time, the honeycomb lattice retains its integrity without breaking in small particles. In this context, the contribution of chemical exfoliation under mild conditions and the organic covalent functionalization is of great importance. In the field of exfoliation of graphite, a common strategy followed is through the use of molecules that are able to penetrate the graphite structure and overcome the strong van der Waals interactions, supporting the multiple graphene layers in graphite, thus leading to stable suspensions.[12−16] Recently, a variety of strategies became also available introducing organic addends covalently attached onto the surface of exfoliated graphene, thus yielding soluble graphene-based materials.[17] Moreover, some novel graphene-based hybrid materials, in which the unique properties of graphene are combined with those of Eu,[18] Au,[19] or CdS[20] nanoparticles as well as photoactive components, such as porphyrins,[21−26] pyrenes,[27−29] and recently electroactive exTTF,[30,31] have been prepared and shown that photoillumination induces intrahybrid charge

Received: June 13, 2012
Revised: August 19, 2012
Published: September 4, 2012

Scheme 1. Covalent Functionalization of Exfoliated Graphene Sheets with ZnPc in *o*-DCB

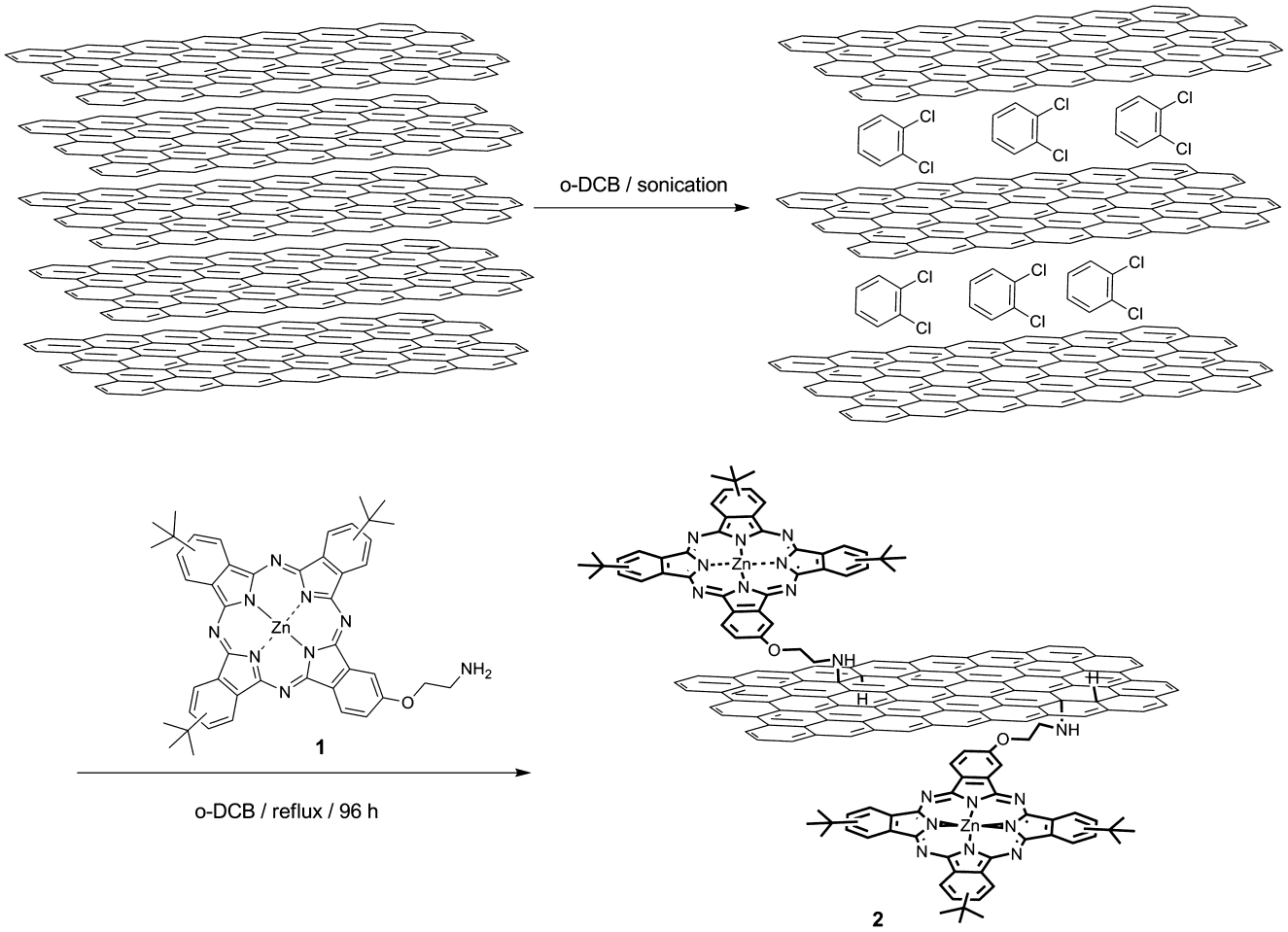

separation. However, none of those materials have been tested so far in energy conversion schemes as active components (i.e., photoanodes) in prototype devices. Actually, the only example in which a graphene-based hybrid material integrated as a component in a photovoltaic cell concerns a supramolecularly interacting zinc phthalocyanine-poly(*p*-phenylene vinylene) with graphene.[32] Therefore, it is absolutely timely to prepare new graphene-based materials and exploit them on the search for advancing the incident photon-to-current conversion efficiency (IPCE).

Phthalocyanines are aromatic macrocycles with a high electronic delocalization and an intense absorption in the red to near-IR zone. They possess a great thermal and photochemical stability and are very versatile, since it is possible to change the central atom and to introduce substituents in the peripheral and axial positions, thus bringing the possibility to tune their physicochemical and optical properties.[33,34] In addition to their applications as photosensitizers for photodynamic therapy,[35,36] as liquid crystals,[37,38] and in nonlinear optics,[39,40] phthalocyanines have emerged with force in the field of photovoltaic devices. They have been used in bulk heterojunction organic solar cells[41−43] and, particularly, in dye-sensitized solar cells (DSSCs),[44−46] as lower-cost and efficient red-absorbing substitutes for standard ruthenium polypyridyl dyes. Recently, there have been substantial increases in power conversion efficiencies in DSSCs using unsymmetrically substituted "push−pull" zinc phthalocyanines with bulky substituents.[47−50] Among them, phthalocyanines have been also covalently and noncovalently connected with different electron acceptor carbon nanostructures,[51,52] such as C_{60},[53−56] $C_{59}N$,[57] carbon nanotubes,[58] and perylenebisimides,[59−66] and the photoinduced electron- and/or energy-transfer properties of these systems have been studied for their use as artificial photosynthetic systems and in organic solar cells.

In the present work, we follow the direct nucleophilic addition[67,68] of primary amines to carbon nanostructured materials for the covalent functionalization of chemically exfoliated graphene, as derived upon ultrasonication treatment with *o*-dichlorobenzene (*o*-DCB), with the custom synthesized (2-aminoethoxy)(tri-*tert*-butyl) zinc phthalocyanine (ZnPc) **1**[60,62,69] (Scheme 1) serving as a light-driven electron donor. The aim of the current research is four-fold, namely, (i) to succeed in the chemical exfoliation of graphene sheets, (ii) to covalently anchor ZnPc dye to exfoliated graphene, (iii) to assess the photophysical properties of the ZnPc−graphene hybrid material, and eventually (iv) to assemble and fabricate the graphene-based hybrid material as a photoanode in a prototype photoelectrochemical cell. The new graphene-based nanohybrid material **2**, in which ZnPc is anchored to the graphitic network through a covalent bond, is rendered soluble in common organic solvents and characterized by complementary spectroscopic, thermal, and microscopy techniques. Furthermore, photoinduced intrahybrid electron-transfer phenomena were investigated and significant photophysical parameters were evaluated. Most importantly, a prototype

dx.doi.org/10.1021/jp305783v | *J. Phys. Chem. C* 2012, 116, 20564−20573

device was constructed by fabricating the graphene-based hybrid material as a photoanode in a photoelectrochemical cell and its efficiency and response were examined. Notably, in the current study, both the presence of the short ethylene chain interconnecting ZnPc with the exfoliated graphene sheet, allowing free rotation and flexibility of the photoactive unit, and the zinc-metalated phthalocyanine itself eventually promoted strong electronic interactions between the two components of the hybrid material to register clearly an efficient photoconversion.

EXPERIMENTAL SECTION

Steady-State Absorption Spectroscopy. The electronic absorption spectra were recorded on a PerkinElmer (Lambda 19) UV−vis-NIR spectrophotometer.

Attenuated Total Reflectance Infrared Spectroscopy. Mid-infrared spectra in the region of 550−4000 cm^{-1} were obtained on a Fourier Transform IR spectrometer (Equinox 55 from Bruker Optics) equipped with a single-reflection diamond ATR accessory (DuraSamp1IR II by SensIR Technologies). A drop of the solution was placed on the diamond surface, followed by evaporation of the solvent, in a stream of nitrogen, before recording the spectrum. Typically, 100 scans were acquired at 4 cm^{-1} resolution.

Raman Spectroscopy. Micro-Raman scattering measurements were performed at room temperature in the backscattering geometry using a Renishaw inVia Raman microscope equipped with a CCD camera and a Leica microscope. A 2400 lines mm^{-1} grating was used for all measurements, providing a spectral resolution of ±1 cm^{-1}. As an excitation source, the Ar^+ laser (514 nm with less than 0.5 mW laser power) was used. Measurements were taken with 60 s of exposure times at varying numbers of accumulations. The laser spot was focused on the sample surface using a long working distance 50× objective. Raman spectra were collected on numerous spots on the sample and recorded with a Peltier cooled CCD camera. The intensity ratio I_D/I_G was obtained by taking the peak intensities following any baseline corrections. The data were collected and analyzed with Renishaw Wire and Origin software.

TEM Analysis. TEM observations were carried out using a JEM-2010F (JEOL) equipped with a CEOS postspecimen spherical aberration corrector (C_s corrector) operating at 120 kV. The ZnPc−graphene specimen was dispersed in *n*-hexane and then fixed on a copper TEM grid coated with holey carbon film.

Atomic Force Microscopy. Atomic force microscopy (AFM) measurements were performed in tapping mode with a Quesant Q-Scope 250 atomic force microscope (Quesant Instrument Co.) equipped with a 40 μm Dual PZT scanner. The images were obtained in ambient conditions with an NSC16 ($W_2CSi_3N_4$) silicon cantilever. Imaging was performed on different scanning areas at a maximum scanning rate of 6 Hz and with image resolution of 600 × 600 pixels in broad-band mode. The microscope was enclosed in an acoustic/thermal isolation unit. For the measurement, a dispersion of 0.2 mg/mL in DMF of the sample was sonicated for 30 min and a few drops were drop-casted on a Si wafer surface. The Si wafer was dried at ambient conditions for 24 h and directly examined with the AFM instrument.

Photoluminescence Spectroscopy. Steady-state emission spectra were recorded on a Fluorolog-3 Jobin Yvon-Spex spectrofluorometer (model GL3-21).

Fluorescence Lifetime. Picosecond time-resolved fluorescence spectra were measured by the time-correlated single-photon counting (TCSPC) method on a NanoLog spectrofluorometer (Horiba Jobin Yvon), using a laser diode as an excitation source (NanoLED, 376 nm, 100 ps pulse width) and by using a streakscope (Hamamatsu Photonics, C5680) as a detector and the laser light (Hamamatsu Photonics M10306, laser diode head, 408 nm) as an excitation source. Lifetimes were evaluated with the DAS6 Fluorescence-Decay Analysis Software.

Femtosecond Laser Flash Photolysis. Femtosecond transient absorption spectroscopy experiments were conducted using an ultrafast source, Integra-C (Quantronix Corp.); an optical parametric amplifier, TOPAS (Light Conversion Ltd.); and a commercially available optical detection system, Helios provided by Ultrafast Systems LLC. The source for the pump and probe pulses was derived from the fundamental output of Integra-C (λ = 786 nm, 2 mJ/pulse, and fwhm = 130 fs) at a repetition rate of 1 kHz. Seventy-five percent of the fundamental output of the laser was introduced into a second harmonic generation (SHG) unit, Apollo (Ultrafast Systems), for excitation light generation at λ = 393 nm, while the rest of the output was used for white light generation. The laser pulse was focused on a sapphire plate of 3 mm in thickness, and then a white light continuum covering the visible region from λ = 410 to 800 nm was generated via self-phase modulation. A variable neutral density filter, an optical aperture, and a pair of polarizers were inserted in the path in order to generate a stable white light continuum. Prior to generating the probe continuum, the laser pulse was fed to a delay line that provides an experimental time window of 3.2 ns with a maximum step resolution of 7 fs. In our experiments, a wavelength at λ = 393 nm of SHG output was irradiated at the sample cell with a spot size of 1 mm in diameter, where it was merged with the white probe pulse in a close angle (<10°). The probe beam after passing through the 2 mm sample cell was focused on a fiber optic cable that was connected to a CMOS spectrograph for recording the time-resolved spectra (λ = 410−1600 nm). Typically, 1500 excitation pulses were averaged for 3 s to obtain the transient spectrum at a set delay time. Kinetic traces at appropriate wavelengths were assembled from the time-resolved spectral data. All measurements were conducted at room temperature.

Photoelectrochemical Measurements. Photoelectrochemical measurements were carried out in a standard two-compartment cell consisting of a working electrode and a Pt wire gauze counter electrode. A Keithley 2400 was used for recording *I*−*V* characteristics and photocurrent generation density under an AM 1.5 simulated light source (OTENTO-SUN II, Bunkoh Keiki Co., LTD). For the IPCE measurements, a monochromator (SM-25, Bunkoh Keiki Co., LTD) was introduced into the path of the excitation beam (150 W xenon lamp, Bunkoh Keiki Co., LTD) for the selected wavelength. The lamp intensity at each wavelength was determined using a Si photodiode (Hamamatsu Photonics S1337-1010BQ) and corrected.

EPR Measurements. A quartz EPR tube (internal diameter: 4.5 mm) containing a deaerated PhCN solution of ZnPc−graphene **2** was irradiated in the cavity of the EPR spectrometer with the focused light of a 1000 W high-pressure Hg lamp (Ushio-USH1005D) through an aqueous filter at low temperature. EPR spectra in frozen cyclohexane were measured under nonsaturating microwave power conditions using a JEOL

dx.doi.org/10.1021/jp305783v | J. Phys. Chem. C 2012, 116, 20564−20573

X-band spectrometer (JES-RE1XE) with an attached variable-temperature apparatus. The magnitude of modulation was chosen to optimize the resolution and the signal-to-noise (S/N) ratio of the observed spectra when the maximum slope line width of the EPR signals was unchanged with a larger modulation magnitude. The g value was calibrated with a Mn^{2+} marker.

Exfoliation of Graphite Flakes. Graphite flakes (200 mg) were placed in a cylindrical vial with 100 mL of *o*-DCB. The mixture was sonicated using a Bandelin Sonoplus Ultrasonic Homogenizer HD 3200 equipped with a flat head probe (VS70T), running at 10% of maximum power (25 W) for 15 min, and then using a Soltec Sonica 3300 ETH-S3 sonic bath for another 2.5 h. The inklike graphene dispersion was centrifuged using an Eppendorf 5702 at 3500 rpm for 15 min, and the supernatant was collected.

Preparation of ZnPc–Graphene Hybrid Material. Exfoliated graphene in *o*-DCB (0.13 mg/mL) was treated with ZnPc **1** (6.8 mg, 8 μmol) at 120 °C for 96 h, and then the mixture was filtered through PTFE (0.1 μm pore size) and washed thoroughly with *o*-DCB, methanol, and dichloromethane. The product (11.2 mg) collected from the top of the filter was found to form a stable inklike dispersion in dichloromethane.

RESULTS AND DISCUSSION

Covalent functionalization of exfoliated graphene sheets is an attractive way of incorporating functional organic moieties with interesting properties directly onto the graphene layer via stable and robust bonds. Especially, when a photoactive unit is added, such covalent attachment can result in more efficient electronic communication of the photoactive moiety with the graphene part, as opposed to noncovalent interactions. Initially, on the basis of that, exfoliation of few-layered graphene sheets from graphite flakes, in the presence of *o*-DCB, was achieved after tip sonication for a limited time period (i.e., 15 min), followed by milder ultrasonication for a longer time (i.e., 2.5 h). Thermal reaction between exfoliated graphene sheets and ZnPc **1**, carrying an alkylamino chain as substituent, then resulted in the nucleophilic addition of phthalocyanine moieties onto the graphene's basal plane, forming ZnPc–graphene **2** (Scheme 1). Hybrid material **2** was found to form black solutions in common organic solvents (i.e., dichloromethane, THF, acetonitrile), and was stable for several weeks, without observing any precipitation, which allowed proceeding with spectroscopic studies in solution.

The exfoliated graphene sheets have an average size (i.e., 650 nm length; 350 nm diameter) and form inklike stable dispersions in *o*-DCB. Morphological evaluation of exfoliated graphene was performed with transmission electron microscopy. Although it is obvious from TEM images that identification of the exact number of exfoliated graphene sheets cannot be accurately measured, the absence of large graphitic particles guarantees the efficiency of the exfoliation protocol followed. The presence of overlapping oligolayered graphene flakes, with typical folding and ripple patterns, being few to several hundred nanometers size in the periphery, is shown in Figure 1a. Imaging of ZnPc–graphene **2** by electron microscopy did not show any alterations on the morphology of the newly formed hybrid material as compared to exfoliated graphene. The particle size distribution of the ZnPc–graphene hybrid material was estimated by dynamic light-scattering measurements as the average diameter for the hybrid material is

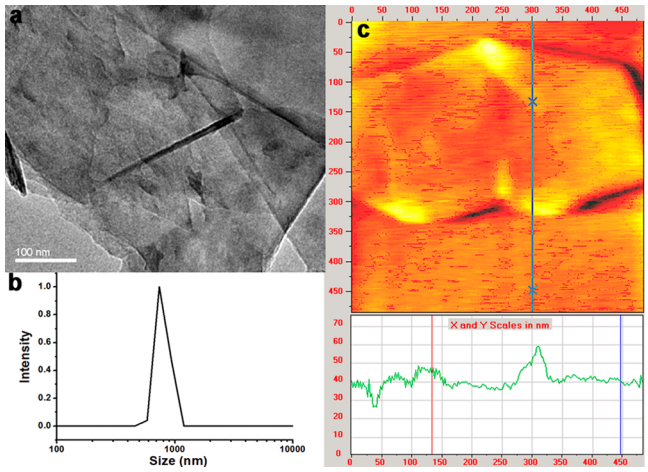

Figure 1. (a) Representative transmission electron micrograph of exfoliated graphene. (b) DLS distribution of ZnPc–graphene hybrid material, obtained in dichloromethane. (c) AFM image of ZnPc–graphene and profile analysis showing a height of 3 nm.

around 750 nm in dichloromethane solution (Figure 1b). Further insight into the nanosized structure of the ZnPc–graphene hybrid material was derived from AFM. When we analyzed several AFM images, graphene sheets reaching almost 0.5 μm in the lateral dimension, with a height of around 3 nm, were found. Considering the height of a single graphene sheet to be less than 1 nm and the added contribution from the attached ZnPc moiety, it is reasonable to expect that the obtained images are representative of single and/or bilayers of ZnPc–graphene sheets (Figure 1c). Obviously, oligolayered graphene sheets were also present.

Raman spectroscopy is a powerful tool for characterizing materials possessing conjugated carbon sp^2-hybridized bonds, such as graphene, due to their intense Raman signals. A detailed micro-Raman spectroscopy characterization was carried out for ZnPc–graphene material **2**, and the corresponding spectrum is shown in Figure 2. The Raman spectrum of exfoliated graphene

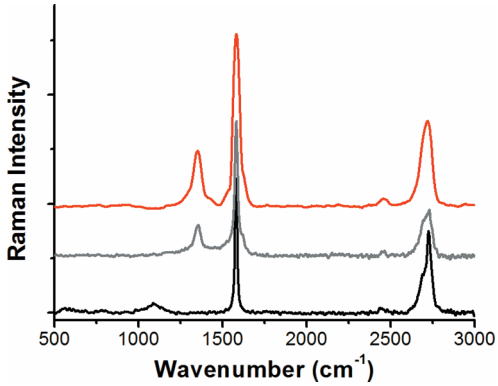

Figure 2. Raman spectra of pristine graphite (black), exfoliated graphene (gray), and ZnPc–graphene hybrid material **2** (red), obtained at λ_{exc} = 514 nm.

shows a D band at 1353 cm^{-1} due to exfoliation, a sharp G band at 1582 cm^{-1} red shifted by ca. 1 cm^{-1} as compared with that of pristine graphite, and a 2D band at 2725 cm^{-1} lowered and broadened as compared with that of intact graphite, proving the existence of exfoliated sheets in the examined sample. The ZnPc–graphene hybrid material **2** shows a similar

dx.doi.org/10.1021/jp305783v | J. Phys. Chem. C 2012, 116, 20564–20573

Raman spectrum with exfoliated graphene, with an enhanced D band (I_D/I_G = 0.35 for **2** vs 0.19 for exfoliated graphene) due to sp^3 carbons generated on the graphitic lattice upon the covalent attachment of ZnPc.

Intact graphite does not show any significant vibrations in the IR spectrum. In contrast, in the attenuated total reflectance IR spectrum of ZnPc–graphene hybrid material **2** (Figure S1 in the Supporting Information), the C–H stretching vibrations due to the ZnPc unit were identified at 2850–2950 cm^{-1}, while the characteristic fingerprint of ZnPc bands were also present at 1045–1610 cm^{-1}, thus, providing significant support for ZnPc covalently bonded onto exfoliated graphene.

The amount of ZnPc covalently anchored onto the graphene lattice was evaluated by thermogravimetric analysis. Pristine graphite is thermally stable under a nitrogen atmosphere up to at least 800 °C. On the other hand, the TGA graph of ZnPc–graphene **2** revealed a 12% weight loss, in the temperature range of 200–500 °C (Figure 3), which is attributed to the

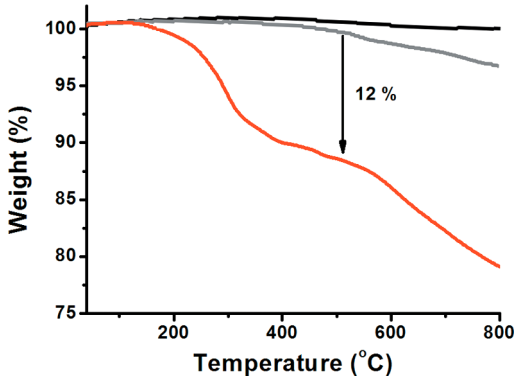

Figure 3. TGA graphs of pristine graphite (black), exfoliated graphene (gray), and ZnPc–graphene **2** (red), obtained under nitrogen.

thermal decomposition of ZnPc covalently attached to graphene sheets. Taking into account that value, the number of graphene carbon atoms per ZnPc unit is estimated, thus giving a functionalization degree of 1 ZnPc per every 518 carbon atoms, in ZnPc–graphene hybrid material **2**. The weight loss that occurred above 500 °C is attributed to the thermal decomposition of defects created at sites where graphene functionalization took place.

Steady-state electronic absorption spectroscopy was used to follow the formation of the ZnPc–graphene hybrid material **2**. In Figure 4, the absorption spectra of ZnPc **1** and ZnPc–graphene **2** in DMF are compared. The absorption spectrum of ZnPc–graphene **2** consists of a broad band centered at 683 nm, followed by smaller absorption bands at 612, and 355 nm assigned to ZnPc, while graphene contributes to the continuing absorption throughout the UV–vis and extending into the NIR region. Compared with reference ZnPc **1**, the absorption of ZnPc in hybrid material **2** is red shifted by 2 nm, has a lower intensity, and appears broadened. These findings based on the optical absorption spectroscopy results not only manifest the efficient formation of ZnPc–graphene but also give sufficient evidence for ground-state electronic interactions between the two species within the hybrid material (even though any aggregation of ZnPc that may take place would also result in a similar observation), similar to other studies based on phthalocyanines covalently grafted to carbon nanotubes.[58,70,71]

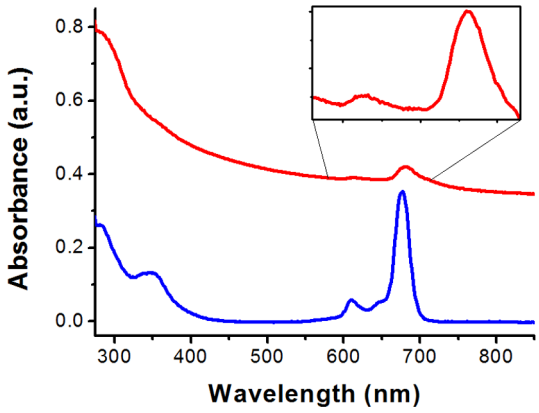

Figure 4. Electronic absorption spectra of ZnPc **1** (blue) and ZnPc–graphene hybrid material **2** (red), obtained in DMF.

Insight into the electronic interplay between ZnPc and graphene in the excited state is derived from photoluminescence studies. Upon excitation at 350 nm, the strong fluorescence emission of ZnPc **1** at 686 nm was significantly quenched by the presence of graphene in the ZnPc–graphene hybrid material **2**, when measurements were performed with matching absorbancies of ZnPc at the excitation wavelength (Figure 5). The latter observation is indicative of electronic

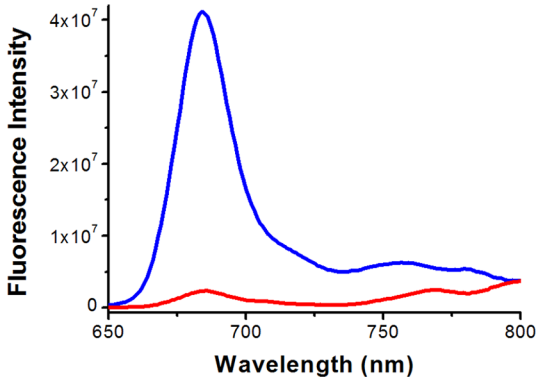

Figure 5. Fluorescence spectra of ZnPc–graphene hybrid material **2** (red) as compared with ZnPc **1** (blue), obtained in DMF. The excitation wavelength was 350 nm, and the concentrations were adjusted so that ZnPc in the two samples exhibited equal absorbance at the excitation wavelength.

interactions between the singlet excited state of zinc phthalocyanine ^{1}(ZnPc)* and graphene, thus suggesting that photoilluminated ZnPc can transport electrons to the electron-accepting graphene sheets, in the ZnPc–graphene hybrid material **2**.

With deeper insight into the excited-state interaction, the ZnPc emission decays of ZnPc–graphene **2** and unbound ZnPc **1** were examined. The charge-transfer interactions between ZnPc and graphene, as documented from the fluorescence quenching for ZnPc in hybrid **2**, should accelerate the decay of the ZnPc emission. Thus, on the basis of the time-correlated single-photon counting (TCSPC) method, the fluorescence lifetime profiles for reference ZnPc **1** were obtained (Figure S2 in the Supporting Information). The analysis of the time profile of the fluorescence decay at 684 nm for the singlet excited state of unbound ZnPc, measured in DMF, was exclusively monoexponentially fitted, with a lifetime of 2.96 ns. However,

dx.doi.org/10.1021/jp305783v | J. Phys. Chem. C 2012, 116, 20564–20573

no fast decaying component of ^{1}ZnPc* in ZnPc–graphene **2**, corresponding to the quenching of the fluorescence intensity in the steady-state spectra, was observed. Implicit is that the singlet excited-state deactivation of ZnPc in **2** is faster than the time resolution of our instrument (i.e., 50 ps). Considering the fast decay value of 50 ps as the upper limit of the actual lifetime attributed to ^{1}ZnPc* in **2**, consistent with the strong emission quenching of ZnPc by graphene as observed in the corresponding steady-state photoluminescence measurement, the minimum value of the rate constant for charge separation (k_{CS}) can then be determined as 1.95×10^{10} s^{-1}. Additionally, the quantum yield for charge separation (Φ_{CS}) is calculated as 0.98.

Time-resolved transient absorption spectra of ZnPc–graphene **2** were measured by femtosecond laser flash photolysis in deaerated PhCN.[72] A transient absorption spectrum observed at 1 ps after laser pulse excitation (λ_{ex} = 393 nm) is shown in Figure 6a. The transient absorption band observed at 1 ps clearly showed the singlet excited state of zinc phthalocyanine ^{1}ZnPc* (λ_{max} = 590 nm),[62,63,73,74] which is overlapped with the strong ground-state bleaching and emission at 680 nm for the ZnPc moiety and vis-NIR region for the graphene entity. As electron transfer from ^{1}ZnPc* to graphene proceeds, the transient absorption due to ^{1}ZnPc* disappears, accompanied by the appearance of the transient absorption band due to ZnPc$^{\bullet+}$. The net change was observed as an increase in bleaching and the red shift of the bleaching peak because of the appearance of the transient absorption at 530 nm due to ZnPc$^{\bullet+}$.[60] Additionally, it has been reported that ZnPc$^{\bullet+}$ also shows an absorption band at 840 nm.[75,76] This band is known to be broadened by strong π–π interactions.[65] Therefore, there was no observation of the absorption band at 840 nm in Figure 6a; together, the red shift and broadening of the absorption band in Figure 4 suggest strong π–π interactions of ZnPc$^{\bullet+}$ with graphene. Although this interpretation has yet to be clearly proven, the time profile of transient absorption at 620 nm clearly consists of two steps (Figure 6b,c),[77] which may well be assigned to the charge separation to form the charge-separated state (ZnPc$^{\bullet+}$–graphene$^{\bullet-}$) and the charge recombination, judging from the observation of the charge-separated state by EPR measurements (vide infra).

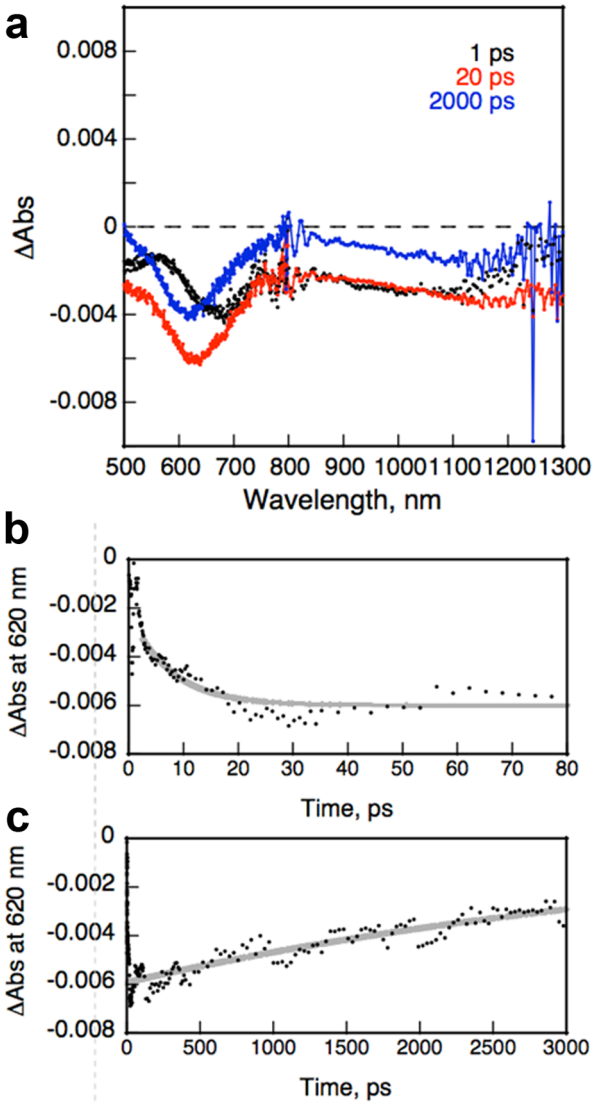

Figure 6. (a) Transient absorption spectra of ZnPc–graphene hybrid material **2** in PhCN observed at 1, 20, and 2000 ps after femtosecond laser excitation (λ = 393 nm). (b) Time profiles of absorbance at 620 nm (b) fast and (c) slow time ranges.

The rate constant of photoinduced electron transfer was determined from monoexponential analysis of the photobleaching time profile at 620 nm (Figure 6b) to be 1.3×10^{11} s^{-1} (lifetime = 7.7 ps).[78] The transient absorption bands of the charge-separated state with bleaching was recovered slowly with the rate constant of 2.3 ($\pm$0.5) $\times$ 10^8 s^{-1} (Figure 6c). The lifetime of the charge-separated state was determined as 4.3 ($\pm$0.8) ns.

To detect the charge-separated state, we measured the EPR spectrum of a PhCN glass containing ZnPc–graphene hybrid material **2** under photoirradiation by a high-pressure Hg lamp (λ > 340 nm) at 77 K. The infrared region was cut off by using a water filter to avoid thermal decomposition of **2**. A single EPR spectrum was observed at g = 2.0028 (Figure 7). This g value agrees well with that of ZnPc$^{\bullet+}$ (2.003),[79,80] which is clearly different from that observed in mechanically exfoliated graphene (2.0045).[81] No signal of the graphene radical anion was observed under the present experimental conditions because the graphene radical anion may have a very broad signal to be detected or disproportionate between two graphene radical anions on the same sheet to generate diamagnetic species.[82–85]

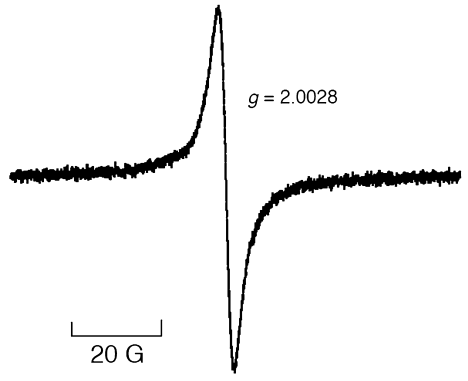

Figure 7. EPR spectrum observed under photoirradiation of a deaerated PhCN glass of ZnPc–graphene hybrid material **2** at 77 K.

dx.doi.org/10.1021/jp305783v | J. Phys. Chem. C 2012, 116, 20564–20573

The photoelectrochemical properties of ZnPc–graphene **2** were evaluated by fabricating thin films of ZnPc–graphene **2** onto nanostructured SnO_2 onto an optical transparent electrode (OTE) by electrophoretic deposition. A suspension of ZnPc–graphene **2** in THF (~2 mL) was transferred into a cuvette, in which the two electrodes OTE and OTE/SnO_2 were placed and kept at a 5 cm distance by a Teflon spacer. Application of a dc electric field (~100 V/cm) resulted in the deposition of ZnPc–graphene **2** from the suspension to the electrode surface and the formation of a robust thin film of OTE/SnO_2/ZnPc–graphene, as documented by discoloration of the suspension and the simultaneous coloration of the OTE/SnO_2 electrode. For reference purposes, a thin film of only graphene, in the absence of ZnPc, was analogously deposited onto the electrode surface to form OTE/SnO_2/graphene. Steady-state electron absorption spectroscopy was used to follow the deposition of the ZnPc–graphene hybrid material onto the electrode surface. In the UV–vis absorption spectrum of the OTE/SnO_2/ZnPc–graphene electrode (Figure S3 in the Supporting Information), the characteristic ZnPc band is identified at around 610 nm. However, it is found further broadened, as compared with the corresponding band in ZnPc–graphene **2** in solution (cf. Figure 4), most likely due to aggregation of ZnPc moieties and/or electronic interactions between ZnPc and graphene. On the other hand, the OTE/SnO_2/graphene electrode shows continuous featureless absorbance in the visible region due to graphene, mirroring the observation registered in solution.

Photoelectrochemical measurements were performed in a standard two-compartment cell, in acetonitrile containing 0.5 M LiI and 0.01 M I_2 as the redox electrolyte and OTE/SnO_2/ZnPc–graphene as the working electrode, while Pt wire was the counter electrode.[86−90] The photocurrent response of the OTE/SnO_2/ZnPc–graphene electrode obtained under white light illumination (AM 1.5 condition; input power = 100 mW·cm^{-2}) is presented in Figure 8. Evidently, the response

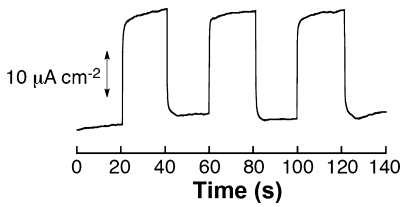

Figure 8. Photocurrent responses of OTE/SnO_2/ZnPc–graphene under white light illumination (AM 1.5 condition). Input power: 100 mW·cm^{-2}.

was found to be prompt, steady, and reproducible during repeated on/off cycles of the visible light illumination. A short-circuit photocurrent density (I_{sc}) of 20 μA·cm^{-2} was measured following the excitation of the OTE/SnO_2/ZnPc–graphene electrode, while blank experiments conducted with OTE/SnO_2 produced no detectable photocurrent under similar experimental conditions.

Moreover, the photocurrent action spectrum of the OTE/SnO_2/ZnPc–graphene electrode was evaluated and compared with that of OTE/SnO_2/graphene (Figure 9), by examining the wavelength dependence of the incident photon-to-current conversion efficiency (IPCE). The IPCE values were calculated by normalizing the photocurrent densities for incident light energy intensity using the following equation[91−93]

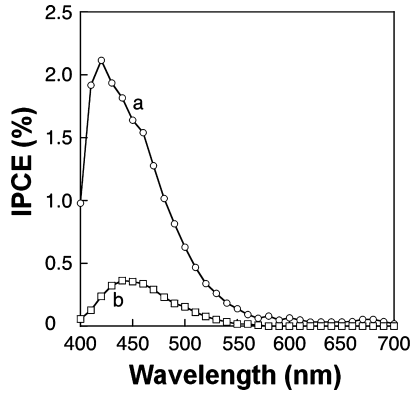

Figure 9. Photocurrent action spectra of (a) OTE/SnO_2/ZnPc–graphene and (b) OTE/SnO_2/graphene (two-electrode system). Electrolyte: 0.5 M LiI and 0.01 M I_2 in acetonitrile.

$$\text{IPCE}\ (\%) = 100 \times 1240 \times I_{sc}/(W_{in} \times \lambda)$$

where I_{sc} is the short-circuit photocurrent (A·cm^{-2}), W_{in} is the incident light intensity (W·cm^{-2}), and λ is the wavelength in nm. Thus, the photocurrent action spectrum of the OTE/SnO_2/ZnPc–graphene electrode, recorded by using a standard two-compartment cell equipped with a potentiostat, shows an IPCE value of 2.2% at 420 nm, which is almost 1 order of magnitude higher than the corresponding value for the OTE/SnO_2/graphene electrode, under the same experimental conditions (Figure 9).[93]

In this context, the anodic photocurrent observed for OTE/SnO_2/ZnPc–graphene films indicates electron transfer from the photoexcited ZnPc to graphene and highlights the significance of excited-state interactions between ZnPc and graphene in hybrid material **2** for generating a photoelectrochemical effect.

In brief, the process responsible for the photocurrent generation includes electron transfer from the photoexcited ZnPc to exfoliated graphene, followed by electron mediation from the reduced graphene layers to the conduction band of the SnO_2 electrode. Importantly, it is worth mentioning that an IPCE value of only 0.3% was registered for noncovalently interacting ZnPc with graphene,[32] thus highlighting the significant role of having the ZnPc anchored through a stable and robust bond onto the graphene sheet, for enhancing photoinduced intrahybrid electron-transfer phenomena between the two components and achieving higher IPCE values.

■ CONCLUSION

Graphene sheets were exfoliated with the aid of sonication in *o*-DCB. Zinc phthalocyanine (ZnPc) was then covalently anchored onto exfoliated graphene, forming electron donor–acceptor ZnPc–graphene hybrid material **2**. The new hybrid material **2** was thoroughly characterized with spectroscopic, thermal, and microscopy techniques. On the basis of absorption studies, ground-state intrahybrid electronic interactions were found to exist, leading to the red shift and broadening of the characteristic absorption bands of ZnPc in hybrid material **2**, as compared with the corresponding absorption features of reference ZnPc **1**. In addition, steady-state fluorescence emission measurements revealed efficient quenching of the characteristic ZnPc emission in hybrid material **2**, suggesting the presence of electronic interactions in the excited states. The dynamics of the system were studied by complementary means,

including time-resolved fluorescence spectroscopy, femtosecond transient absorption spectroscopy, and EPR, thus revealing charge separation generating $ZnPc^{\bullet+}$–$graphene^{\bullet-}$ via the singlet excited state of ZnPc. Finally, a photoelectrochemical cell based on the fabrication of ZnPc–graphene as a photoanode onto an optical transparent electrode (OTE) cast with nanostructured SnO_2 films (OTE/SnO_2) was constructed. The film of the OTE/SnO_2/ZnPc–graphene electrode revealed prompt, stable, and reproducible photocurrent, while the IPCE value was measured. Overall, this is a promising and leading initiative for hybrid materials combining graphene and photoactive moieties for applications in solar cells.

■ ASSOCIATED CONTENT

Supporting Information

ATR-IR of ZnPc and ZnPc–graphene, fluorescence decay profile of ZnPc, and absorption spectra of OTE/SnO_2/ZnPc–graphene film. This material is available free of charge via the Internet at http://pubs.acs.org.

■ AUTHOR INFORMATION

Corresponding Author

*E-mail: tagmatar@eie.gr (N.T.), asastre@umh.es (Á.S.-S.), hasobe@chem.keio.ac.jp (T.H.), fukuzumi@chem.eng.osaka-u.ac.jp (S.F.).

Author Contributions

The manuscript was written through contributions of all authors. All authors have given approval to the final version of the manuscript.

Notes

The authors declare no competing financial interest.

■ ACKNOWLEDGMENTS

Partial financial support from GSRT/NSRF 2007-2013, the actions "Cooperation" through Project 09ΣΥΝ-42-691, and "Postdoctoral support" Project GRAPHCELL PE5(2126) as well as COST network MP0901 NanoTP to N.T. is acknowledged. This work was also partially supported by Grant-in-Aids for Scientific Research (Nos. 23108721 and 23681025 to T.H., No. 20108010 to S.F., No. 23750014 to K.O.), MEXT-Supported Program for the Strategic Research Foundation at Private Universities, 2009-2013, and a WCU project (R31-2008-000-10010-0) through KOSEF/MEST, Korea. Grants Consolider-Ingenio 2010 project HOPE CSD2007-00007, PROMETEO 2012/010 and CTQ2011-26455 from GVA, MINECO and FEDER, to A.S.-S. are acknowledged.

■ REFERENCES

(1) Novoselov, K. S.; Geim, A. K.; Morozov, S. V.; Jiang, D.; Zhang, Y.; Dubonos, S. V.; Grigorieva, I. V.; Firsov, A. A. *Science* **2004**, *306*, 666–669.
(2) Geim, A. K.; Novoselov, K. S. *Nat. Mater.* **2007**, *6*, 183–191.
(3) Nair, R. R.; Blake, P.; Grigorenko, A. N.; Novoselov, K. S.; Booth, T. J.; Stauber, T.; Peres, N. M. R.; Geim, A. K. *Science* **2008**, *320*, 1308–1308.
(4) Lee, C.; Wei, X.; Kysar, J. W.; Hone, J. *Science* **2008**, *321*, 385–388.
(5) Novoselov, K. S.; Jiang, D.; Schedin, F.; Booth, T. J.; Khotkevich, V. V.; Morozov, S. V.; Geim, A. K. *Proc. Natl. Acad. Sci. U.S.A.* **2005**, *102*, 10451–10453.
(6) Novoselov, K. S.; Geim, A. K.; Morozov, S. V.; Jiang, D.; Katsnelson, M. I.; Grigorieva, I. V.; Dubonos, S. V.; Firsov, A. A. *Nature* **2005**, *438*, 197–200.
(7) Morozov, S. V.; Novoselov, K. S.; Katsnelson, M. I.; Schedin, F.; Elias, D. C.; Jaszczak, J. A.; Geim, A. K. *Phys. Rev. Lett.* **2008**, *100*, 016602–016605.
(8) Bai, H.; Li, C.; Shi, G. *Adv. Mater.* **2011**, *23*, 1089–1115.
(9) Kamat, P. V. *J. Phys. Chem. Lett.* **2011**, *2*, 242–251.
(10) Loh, K. P.; Bao, Q.; Ang, P. K.; Yang, J. *J. Mater. Chem.* **2010**, *20*, 2277–2289.
(11) Dreyer, D. R.; Park, S.; Bielawski, C. W.; Ruoff, R. S. *Chem. Soc. Rev.* **2010**, *39*, 228–240.
(12) Hernandez, Y.; Nicolosi, V.; Lotya, M.; Blighe, F. M.; Sun, Z.; De, S.; McGovern, I. T.; Holland, B.; Byrne, M.; Gun'Ko, Y. K.; et al. *Nat. Nanotechnol.* **2008**, *3*, 563–568.
(13) Hamilton, C. E.; Lomeda, J. R.; Sun, Z.; Tour, J. M.; Barron, A. R. *Nano Lett.* **2009**, *9*, 3460–3462.
(14) Coleman, J. N. *Adv. Funct. Mater.* **2009**, *19*, 3680–3695.
(15) Behabtu, N.; Lomeda, J. R.; Green, M. J.; Higginbotham, A. L.; Sinitskii, A.; Kosynkin, D. V.; Tsentalovich, D.; Parra-Vasquez, A. N. G.; Schmidt, J.; Kesselman, E.; et al. *Nat. Nanotechnol.* **2010**, *5*, 406–411.
(16) Lotya, M.; King, P. J.; Khan, U.; De, S.; Coleman, J. N. *ACS Nano* **2010**, *4*, 3155–3162.
(17) Yan, X.; Li, L.-s. *J. Mater. Chem.* **2011**, *21*, 3295–3300.
(18) Gupta, B. K.; Thanikaivelan, P.; Narayanan, T. N.; Song, L.; Gao, W.; Hayashi, T.; Leela Mohana Reddy, A.; Saha, A.; Shanker, V.; Endo, M.; et al. *Nano Lett.* **2011**, *11*, 5227–5233.
(19) Goncalves, G.; Marques, P. A. A. P.; Granadeiro, C. M.; Nogueira, H. I. S.; Singh, M. K.; Grácio, J. *Chem. Mater.* **2009**, *21*, 4796–4804.
(20) Cao, A.; Liu, Z.; Chu, S.; Wu, M.; Ye, Z.; Cai, Z.; Chang, Y.; Wang, S.; Gong, Q.; Liu, Y. *Adv. Mater.* **2010**, *22*, 103–106.
(21) Xu, Y.; Liu, Z.; Zhang, X.; Wang, Y.; Tian, J.; Huang, Y.; Ma, Y.; Zhang, X.; Chen, Y. *Adv. Mater.* **2009**, *21*, 1275–1279.
(22) Karousis, N.; Economopoulos, S. P.; Sarantopoulou, E.; Tagmatarchis, N. *Carbon* **2010**, *48*, 854–860.
(23) Tu, W.; Lei, J.; Zhang, S.; Ju, H. *Chem.—Eur. J.* **2010**, *16*, 10771–10777.
(24) Karousis, N.; Sandanayaka, A. S. D.; Hasobe, T.; Economopoulos, S. P.; Sarantopoulou, E.; Tagmatarchis, N. *J. Mater. Chem.* **2011**, *21*, 109–117.
(25) Wang, H.-X.; Zhou, K.-G.; Xie, Y.-L.; Zeng, J.; Chai, N.-N.; Li, J.; Zhang, H.-L. *Chem. Commun.* **2011**, *47*, 5747–5749.
(26) Zhang, X.; Hou, L.; Cnossen, A.; Coleman, A. C.; Ivashenko, O.; Rudolf, P.; van Wees, B. J.; Browne, W. R.; Feringa, B. L. *Chem.—Eur. J.* **2011**, *17*, 8957–8964.
(27) An, X.; Simmons, T.; Shah, R.; Wolfe, C.; Lewis, K. M.; Washington, M.; Nayak, S. K.; Talapatra, S.; Kar, S. *Nano Lett.* **2010**, *10*, 4295–4301.
(28) An, X.; Butler, T. W.; Washington, M.; Nayak, S. K.; Kar, S. *ACS Nano* **2011**, *5*, 1003–1011.
(29) Mann, J. A.; Rodríguez-López, J.; Abruña, H. D.; Dichtel, W. R. *J. Am. Chem. Soc.* **2011**, *133*, 17614–17617.
(30) Das, B.; Voggu, R.; Rout, C. S.; Rao, C. N. R. *Chem. Commun.* **2008**, 5155–5157.
(31) Economopoulos, S. P.; Rotas, G.; Miyata, Y.; Shinohara, H.; Tagmatarchis, N. *ACS Nano* **2010**, *4*, 7499–7507.
(32) Malig, J.; Jux, N.; Kiessling, D.; Cid, J.-J.; Vázquez, P.; Torres, T.; Guldi, D. M. *Angew. Chem., Int. Ed.* **2011**, *50*, 3561.
(33) de la Torre, G.; Claessens, C. G.; Torres, T. *Chem. Commun.* **2007**, 2000–2002.
(34) Leznoff, C. C., Lever, A. B. P., Eds. *Phthalocyanines: Properties and Applications*; VCH Publishers: New York, 1990–1996; Vol. *1–4*.
(35) Ben-Hur, E.; Chan, W.-S. Phthalocyanines in Photobiology and Their Medical Applications. In *The Porphyrin Handbook*; Kadish, K. M., Smith, K. M., Guilard, R., Eds.; Academic Press: Boston, MA, 2003; Vol. *19*, pp 1–35.
(36) Ali, H.; van Lier, J. E. *Chem. Rev.* **1999**, *99*, 2379–2450.

(37) Ince, M.; Martínez-Díaz, M. V.; Barberá, J.; Torres, T. J. *Mater. Chem.* **2011**, *21*, 1531−1536.
(38) Hayashi, H.; Nihashi, W.; Umeyama, T.; Matano, Y.; Seki, S.; Shimizu, Y.; Imahori, H. *J. Am. Chem. Soc.* **2011**, *133*, 10736−10739.
(39) de la Torre, G.; Vázquez, P.; Agulló-López, F.; Torres, T. *Chem. Rev.* **2004**, *104*, 3723−3750.
(40) Chen, Y.; Hanack, M.; Blau, W. J.; Dini, D.; Liu, Y.; Lin, Y.; Bai, J. *J. Mater. Sci.* **2006**, *41*, 2169−2185.
(41) Fischer, M. K. R; López-Duarte, I.; Wienk, M. M.; Martínez-Díaz, M. V.; Janssen, R. A. J.; Bauerle, P.; Torres, T. *J. Am. Chem. Soc.* **2009**, *131*, 8669−8676.
(42) Varotto, A.; Nam, C.-Y.; Radivojevioc, I.; Tomé, J. P. C.; Cavaleiro, J. A. S.; Black, C. T.; Drain, C. M. *J. Am. Chem. Soc.* **2010**, *132*, 2552−2554.
(43) Lee, J. U.; Kim, Y. D.; Jo, J. W.; Kim, J. P.; Jo, W. H. *J. Mater. Chem.* **2011**, *21*, 17209−17218.
(44) Grätzel, M. *Acc. Chem. Res.* **2009**, *42*, 1788−1798.
(45) Barea, E. M.; Ortiz, J.; Paya, F. J.; Fernández-Lázaro, F.; Fabregat-Santiago, F.; Sastre-Santos, A.; Bisquert, J. *Energy Environ. Sci.* **2010**, *3*, 1985−1994.
(46) Martínez-Díaz, M. V.; Ince, M.; Torres, T. *Monatsh. Chem.* **2011**, *142*, 699−707.
(47) Cid, J. J.; Yum, J. H.; Jang, S. R.; Nazeeruddin, M. K.; Martínez-Ferrero, E.; Palomares, E.; Ko, J.; Grätzel, M.; Torres, T. *Angew. Chem., Int. Ed.* **2007**, *46*, 8358−8362.
(48) Mori, S.; Nagata, M.; Nakahata, Y.; Yasuta, K.; Goto, R.; Kimura, M.; Taya, M. *J. Am. Chem. Soc.* **2010**, *132*, 4054−4055.
(49) Ragoussi, M.-E.; Cid, J.-J.; Yum, J.-H.; de la Torre, G.; di Censo, D.; Grätzel, M.; Nazeeruddin, M. K.; Torres, T. *Angew. Chem., Int. Ed.* **2012**, *51*, 4375−4378.
(50) García-Iglesias, M.; Yum, J. H.; Humphry-Baker, R.; Zakeeruddin, S. M.; Pechy, P.; Vázquez, P.; Palomares, E.; Grätzel, M.; Nazeeruddin, M. K.; Torres, T. *Chem. Sci.* **2011**, *2*, 1145−1150.
(51) Elemans, J. A. A. W.; van Hameren, R.; Nolte, R. J. M.; Rowan, A. E. *Adv. Mater.* **2006**, *18*, 1251−1266.
(52) Bottari, G.; de la Torre, G.; Guldi, D. M.; Torres, T. *Chem. Rev.* **2010**, *110*, 6768−6816.
(53) Sastre, A.; Gouloumis, A.; Vazquez, P.; Torres, T.; Doan, V.; Schwartz, B. J.; Wudl, F.; Echegoyen, L.; Rivera, J. *Org. Lett.* **1999**, *1*, 1807−1810.
(54) Gouloumis, A.; Liu, S. G.; Sastre, A.; Vazquez, P.; Echegoyen, L.; Torres, T. *Chem.—Eur. J.* **2000**, *6*, 3600−3607.
(55) Martin-Gomis, L.; Ohkubo, K.; Fernandez-Lazaro, F.; Fukuzumi, S.; Sastre-Santos, A. *Org. Lett.* **2007**, *9*, 3441−3444.
(56) Pinzón, J. R.; Cardona, C. M.; Herranz, M. A.; Plonska-Brzezinska, M. E.; Palkar, A.; Athans, A. J.; Martín, N.; Rodríguez-Fortea, A.; Poblet, J. M.; Bottari, G.; et al. *Chem.—Eur. J.* **2009**, *15*, 864−877.
(57) Rotas, G.; Ranta, J.; Efimov, A.; Niemi, M.; Lemmetyinen, H.; Tkachenko, N.; Tagmatarchis, N. *ChemPhysChem* **2012**, *13*, 1246−1254.
(58) Campidelli, S.; Ballesteros, B.; Filoramo, A.; Díaz Díaz, D.; de la Torre, G.; Torres, T.; Rahman, G. M. A.; Ehli, C.; Kiessling, D.; Werner, F.; et al. *J. Am. Chem. Soc.* **2008**, *130*, 11503−11509.
(59) Li, X.; Sinks, L. E.; Rybtchinski, B.; Wasielewski, M. R. *J. Am. Chem. Soc.* **2004**, *126*, 10810−10811.
(60) Fukuzumi, S.; Ohkubo, K.; Ortiz, J.; Gutiérrez, A. M.; Fernández-Lázaro, F.; Sastre-Santos, A. *Chem. Commun.* **2005**, 3814−3816.
(61) Rodríguez-Morgade, M. S.; Torres, T.; Atienza-Castellanos, C.; Guldi, D. M. *J. Am. Chem. Soc.* **2006**, *128*, 15145−15154.
(62) Fukuzumi, S.; Ohkubo, K.; Ortiz, J.; Gutiérrez, A. M.; Fernández-Lázaro, F.; Sastre-Santos, A. *J. Phys. Chem. A* **2008**, *112*, 10744−10752.
(63) Céspedes-Guirao, F. J.; Ohkubo, K.; Fukuzumi, S.; Sastre-Santos, Á.; Fernández-Lázaro, F. *J. Org. Chem.* **2009**, *74*, 5871−5880.
(64) Albert-Seifried, S.; Finlayson, C. E.; Laquai, F.; Friend, R. H.; Swager, T. M.; Kouwer, P. H. J.; Juríček, M.; Kitto, H. J.; Valster, S.; Nolte, R. J. M.; et al. *Chem.—Eur. J.* **2010**, *16*, 10021−10029.
(65) Céspedes-Guirao, F. J.; Martín-Gomis, L.; Ohkubo, K.; Fukuzumi, S.; Fernández-Lázaro, F; Sastre-Santos, Á. *Chem.—Eur. J.* **2011**, *17*, 9153−9163.
(66) Céspedes-Guirao, F. J.; Ohkubo, K.; Fukuzumi, S.; Fernández-Lázaro, F.; Sastre-Santos, Á. *Chem.—Asian J.* **2011**, *11*, 3110−3121.
(67) Basiuk, E. V.; Monroy-Peláez, M.; Puente-Lee, I.; Basiuk, V. A. *Nano Lett.* **2004**, *4*, 863−866.
(68) Cioffi, C.; Campidelli, S.; Sooambar, C.; Marcaccio, M.; Marcolongo, G.; Meneghetti, M.; Paolucci, D.; Paolucci, F.; Ehli, C.; Rahman, G. M. A.; et al. *J. Am. Chem. Soc.* **2007**, *129*, 3938−3945.
(69) Sibrian-Vazquez, M.; Ortiz, J.; Nesterova, I. V.; Fernández-Lázaro, F.; Sastre-Santos, Á.; Soper, S. A.; Vicente, M. G. H. *Bioconjugate Chem.* **2007**, *18*, 410−420.
(70) Mugadza, T.; Nyokong, T. *Synth. Met.* **2010**, *160*, 2089−2098.
(71) Chidawanyika, W.; Nyokong, T. *Carbon* **2010**, *48*, 2831−2338.
(72) The femtosecond laser flash photolysis measurements were also carried out in DMF (ε_s = 36.7), which is more polar than PhCN (ε_s = 25.2). However, we could not detect the charge-separated state probably because of the much faster decay of the charge-separated state in DMF than in PhCN. The driving force of charge recombination in DMF will be smaller than that in PhCN, which may result in acceleration of the charge recombination in the Marcus inverted region; see: Imahori, H.; Tamaki, K.; Guldi, D. M.; Luo, C.; Fujitsuka, M.; Ito, O.; Sakata, Y.; Fukuzumi, S. *J. Am. Chem. Soc.* **2001**, *123*, 2607−2617.
(73) Jiménez, A. J.; Spänig, F.; Rodríguez-Morgade, M. S.; Ohkubo, K.; Fukuzumi, S.; Guldi, D. M.; Torres, T. *Org. Lett.* **2007**, *9*, 2481−2484.
(74) Blas-Ferrando, V. M.; Ortiz, J.; Bouissane, L.; Ohkubo, K.; Fukuzumi, S.; Fernández-Lázaro, F.; Sastre-Santos, Á. *Chem. Commun.* **2012**, *48*, 6241−6243.
(75) Guldi, D. M.; Zilbermann, I.; Gouloumis, A.; Vázquez, P.; Torres, T. *J. Phys. Chem. B* **2004**, *108*, 18485−18494.
(76) Supur, M.; Yamada, Y.; El-Khouly, M. E.; Honda, T.; Fukuzumi, S. *J. Phys. Chem. C* **2011**, *115*, 15040−15047.
(77) The time profile of transient absorption at 620 nm was recorded to determine the rate constants because the absorption change is maximum at 620 nm.
(78) The lifetime of **2** is much shorter than the fluorescence lifetime (∼150 ps) expected from the strong fluorescence quenching (∼5%) and the fluorescence lifetime of **1** (∼3 ns). However, the quantitative discussion on the quenching efficiency is difficult because the small portion of ZnPc that is not attached to graphene results in fluorescence.
(79) Fu, Y.; Fu, G.; Lever, A. B. P. *Inorg. Chem.* **1994**, *33*, 1038−1044.
(80) Niemi, M.; Tkachenko, N. V.; Efimov, A.; Lehtivouori, H.; Ohkubo, K.; Fukuzumi, S.; Lemmetyinen, H. *J. Phys. Chem. A* **2008**, *112*, 6884−6892.
(81) Ciric, L.; Sienkiewicz, A.; Náfrádi, B.; Mionic, M.; Magrez, A.; Forró, L. *Phys. Status Solidi B* **2009**, *246*, 2558−2561.
(82) Saito, K.; Ohtani, M.; Fukuzumi, S. *J. Am. Chem. Soc.* **2006**, *128*, 14216−14217.
(83) Saito, K.; Ohtani, M.; Fukuzumi, S. *Chem. Commun.* **2007**, 55−57.
(84) Ohtani, M.; Saito, K.; Fukuzumi, S. *Chem.—Eur. J.* **2009**, *15*, 9160−9168.
(85) Kojima, T.; Nakanishi, T.; Harada, R.; Ohkubo, K.; Yamauchi, S.; Fukuzumi, S. *Chem.—Eur. J.* **2007**, *13*, 8714−8725.
(86) Pagona, G.; Sandanayaka, A. S. D.; Hasobe, T.; Charalambidis, G.; Coutsolelos, A. G.; Yudasaka, M.; Iijima, S.; Tagmatarchis, N. *J. Phys. Chem. C* **2008**, *112*, 15735−15741.
(87) Vizuete, M.; Gomez-Escalonilla, M. J.; Fierro, J. L. G.; Sandanayaka, A. S. D.; Hasobe, T.; Yudasaka, M.; Iijima, S.; Ito, O.; Langa, F. *Chem.—Eur. J.* **2010**, *16*, 10752−10763.
(88) Kongkanand, A.; Tvrdy, K.; Takechi, K.; Kuno, M.; Kamat, P. V. *J. Am. Chem. Soc.* **2008**, *130*, 4007−4015.
(89) Kamat, P. V. *J. Phys. Chem. C* **2008**, *112*, 18737−18753.

(90) Lee, H. J.; Yum, J. H.; Leventis, H. C.; Zakeeruddin, S. M.; Haque, S. A.; Chen, P.; Seok, S. I.; Grätzel, M.; Nazeeruddin, M. K. *J. Phys. Chem. C* **2008**, *112*, 11600−11608.
(91) Hasobe, T.; Kashiwagi, Y.; Absalom, M. A.; Sly, J.; Hosomizu, K.; Crossley, M. J.; Imahori, H.; Kamat, P. V.; Fukuzumi, S. *Adv. Mater.* **2004**, *16*, 975−979.
(92) Hasobe, T.; Kamat, P. V.; Absalom, M. A.; Kashiwagi, Y.; Sly, J.; Crossley, M. J.; Hosomizu, K.; Imahori, H.; Fukuzumi, S. *J. Phys. Chem. B* **2004**, *108*, 12865−12872.
(93) The main reason for the difference between IPCE (Figure 9) and absorption (Figure S3, Supporting Information) spectra is due to the measurement setup in the electrolyte system (SnO_2 nanocrystallites and I^-/I_3^- redox couple in acetonitrile) since the incident light is absorbed by the electrolyte solution and SnO_2 nanocrystallites in the short-wavelength region. In the long-wavelength region, the large scattering or aggregate trend may have an effect on the low IPCE value. See the following related papers: (a) Hasobe, T.; Fukuzumi, S.; Kamat, P. V. *J. Phys. Chem. B* **2006**, *110*, 25477−25484. (b) Hasobe, T.; Fukuzumi, S.; Kamat, P. V. *Angew. Chem., Int. Ed.* **2006**, *45*, 755−759.
(94) Ragoussi, M.-E.; Malig, J.; Katsukis, G.; Butz, B.; Spiecker, E.; de la Torre, G.; Torres, T.; Guldi, D. M. *Angew. Chem., Int. Ed.* **2012**, *51*, 6421−6425.

NOTE ADDED IN PROOF

During the submission of the current work, we noticed that a similar hybrid material in which metal-free phthalocyanine condensed through a long bridge onto pyrrolidine-functionalized graphene was just synthesized and showed the formation of charge-separated states upon photoirradiation.[94]